


RESEARCH ARTICLE

Open Access

Neuroprotection by *Wld^S* depends on retinal ganglion cell type and age in glaucoma



Michael L. Risner[†], Silvia Pasini[†], Nolan R. McGrady, Karis B. D'Alessandro, Vincent Yao, Melissa L. Cooper and David J. Calkins^{*} 

Abstract

Background: Early challenges to axonal physiology, active transport, and ultrastructure are endemic to age-related neurodegenerative disorders, including those affecting the optic nerve. Chief among these, glaucoma causes irreversible vision loss through sensitivity to intraocular pressure (IOP) that challenges retinal ganglion cell (RGC) axons, which comprise the optic nerve. Early RGC axonopathy includes distal to proximal progression that implicates a slow form of Wallerian degeneration. In multiple disease models, including inducible glaucoma, expression of the slow *Wallerian degeneration* (*Wld^S*) allele slows axon degeneration and confers protection to cell bodies.

Methods: Using an inducible model of glaucoma along with whole-cell patch clamp electrophysiology and morphological analysis, we tested if *Wld^S* also protects RGC light responses and dendrites and, if so, whether this protection depends upon RGC type. We induced glaucoma in young and aged mice to determine if neuroprotection by *Wld^S* on anterograde axonal transport and spatial contrast acuity depends on age.

Results: We found *Wld^S* protects dendritic morphology and light-evoked responses of RGCs that signal light onset (α ON-Sustained) during IOP elevation. However, IOP elevation significantly reduces dendritic complexity and light responses of RGCs that respond to light offset (α OFF-Sustained) regardless of *Wld^S*. As expected, *Wld^S* preserves anterograde axon transport and spatial acuity in young adult mice, but its protection is significantly limited in aged mice.

Conclusion: The efficacy of *Wld^S* in conferring protection to neurons and their axons varies by cell type and diminishes with age.

Keywords: Slow Wallerian degeneration, *Wld^S*, Neuroprotection, Neurodegeneration, Glaucoma, Retinal ganglion cells, Axonopathy, Dendritic morphology

* Correspondence: david.j.calkins@vumc.org

[†]Michael L. Risner and Silvia Pasini contributed equally to this work.
Department of Ophthalmology and Visual Sciences, Vanderbilt Eye Institute,
Vanderbilt University Medical Center, AA7103 MCN/VUIIS, 1161 21st Ave. S,
Nashville, TN 37232, USA



© The Author(s). 2021 **Open Access** This article is licensed under a Creative Commons Attribution 4.0 International License, which permits use, sharing, adaptation, distribution and reproduction in any medium or format, as long as you give appropriate credit to the original author(s) and the source, provide a link to the Creative Commons licence, and indicate if changes were made. The images or other third party material in this article are included in the article's Creative Commons licence, unless indicated otherwise in a credit line to the material. If material is not included in the article's Creative Commons licence and your intended use is not permitted by statutory regulation or exceeds the permitted use, you will need to obtain permission directly from the copyright holder. To view a copy of this licence, visit <http://creativecommons.org/licenses/by/4.0/>. The Creative Commons Public Domain Dedication waiver (<http://creativecommons.org/publicdomain/zero/1.0/>) applies to the data made available in this article, unless otherwise stated in a credit line to the data.

Background

Age-related neurodegenerative disorders of the brain differ in etiology but often share similar important features [1, 2]. Among these are early challenges to axonal physiology, active transport, and ultrastructure [1, 3]. These pathological features are also endemic in diseases that affect the optic nerve, which conveys visual signals from the retina to central projection sites in the brain. Glaucomatous optic neuropathy (or glaucoma) is characterized by early axonopathy, including deficits in axonal anterograde transport from retina to central brain targets [4, 5]. The disease causes vision loss through progressive degeneration of retinal ganglion cells (RGCs) and their axons, which comprise the optic nerve. The disease remains a prevalent neurodegenerative disorder and is the leading cause of irreversible blindness worldwide, with an estimated 100 million people afflicted by 2040 [6]. Sensitivity to intraocular pressure (IOP) is an associated risk factor for glaucoma, and higher IOP is linked to accelerated pathology [5, 7, 8]. Thus, current treatments focus on lowering IOP. However, regardless of hypotensive therapeutic intervention, many patients continue to lose vision [9]. Thus, like age-related diseases of the brain itself, therapeutics are needed that address neurodegeneration directly [10].

Abating axon dysfunction early in neurodegeneration can prevent subsequent stages of glaucomatous progression [2, 3, 11, 12]. This is so as well in experimental models of glaucoma, which generally rely upon inducible or transgenic-related elevations in IOP [13, 14]. In rodents, experimental interventions that slow or prevent loss of anterograde transport to RGC projection sites in the brain also impede axon degeneration in the optic nerve and cell body loss in the retina [5, 15–17]. Without intact transport, axons undergo Wallerian or Wallerian-like degeneration [1]. Expression of the *Wld^S* (slow Wallerian degeneration) allele significantly delays axon degeneration in numerous disease models [18], though protection is dose- and possibly age-dependent [19, 20]. In glaucoma models, *Wld^S* preserves RGC axon structure, delays cell body loss, and preserves measures of gross retinal function [21–25]. The *Wld^S* mutation creates a chimeric fusion protein containing 70 N-terminal amino acids of ubiquitination factor *Ube4b* linked to full-length nicotinamide mononucleotide adenylyltransferase 1 or *Nmnat1*, the enzyme responsible for synthesis of nicotinamide adenine dinucleotide or NAD, a cofactor involved in oxidative phosphorylation [26–28]. Glaucoma compromises RGC axon metabolism long before outright degeneration primarily through elevated oxidative stress and reduced mitochondrial efficiency [4, 5, 29]. Supplementation with nicotinamide, a NAD precursor, preserves RGC metabolism, anterograde axon transport and optic nerve integrity in the DBA/2J mouse model of glaucoma [24, 30].

Here we asked whether *Wld^S* also confers protection to RGC dendritic arbors in the retina and, if so, whether this protection depends upon RGC type. In glaucoma, RGCs that depolarize to light onset (ON cells) or light offset (OFF cells) may show different susceptibility to IOP elevations [31–33]. Using our microbead occlusion paradigm [14, 29, 34], we elevated IOP (+33%) in *Wld^S* mice and recorded light responses from a major class of ON and OFF RGCs, the α -Sustained type [32, 33, 35, 36]. By comparing wild-type (WT) and *Wld^S* RGC responses and morphology, we find that *Wld^S* protects α ON-Sustained light responses and dendritic morphology following IOP elevation for 1 month. However, *Wld^S* α OFF-Sustained RGCs showed reduced light responses and dendritic complexity, similar to WT RGCs. Interestingly, while *Wld^S* preserved anterograde axonal transport to the brain and spatial contrast acuity in young mice, its protection diminished with age.

Methods

Animals

The Vanderbilt University Institutional Animal Care and Use Committee approved all experimental procedures described below. We purchased 6 to 8-week-old and 1-year old male wild type C57BL/6 mice (WT) from the Charles River Laboratory (Wilmington, MA). Two breeding pairs of homozygous slow Wallerian degeneration mutant mice (*Wld^S*) on C57BL/6 background were kindly donated by Dr. Shu-Wei Sun from Loma Linda University [37]. We bred *Wld^S* mice in the Vanderbilt University Medical Center Division of Animal Care. For our experiments we used 6 to 10-week-old and 1-year old male and female homozygous *Wld^S* mice (see Genotype Confirmation). Mice were maintained on a 12-h light-dark cycle with standard rodent chow available ad libitum.

Genotype confirmation

We genotyped *Wld^S* mice following the published protocol [38]. Briefly, we extracted genomic DNA from tails (DNeasy Blood & Tissue, Qiagen, Hilden, Germany). Because the *Wld^S* mutation contains an in tandem triplication of a region intrinsic to the mouse genome, we determined the copy number of mutant *Wld^S* alleles (QuantStudio 3 Real Time PCR, Applied Biosystems, Waltham, MA) using the following primers: *Wld^S* forward: 5'-GGC AGT GAC GCT CAG AAA TTC-3' and *Wld^S* reverse: 5'-GTT CAC CAG GTG GAT GTT GCT-3'. β -tubulin forward: 5'-GCC AGA GTG GTG CAG GAA ATA-3' β -tubulin reverse: 5'-TCA CCA CGT CCA GGA CAG AGT-3'. For each mouse, *Wld^S* allele copy number was measured in triplicate, normalized to β -tubulin as endogenous control, and we quantified the copy number using the comparative Δ CT method [39]. We then normalized *Wld^S* copy number

relative to *Wld^S* copy number measured in WT C57 mice obtained from Charles River Laboratory. As previously observed [38], *Wld^S* copies formed a continuum. We defined animal genotype by *Wld^S* copies using criteria established by [38]. *Wld^S* null mice copy number ranged from 0 to 1.4 (*Wld^S*^{-/-}), *Wld^S* heterozygotes 1.4–2.5 (*Wld^S*^{+/-}), and *Wld^S* homozygotes ≥ 2.5 (*Wld^S*^{+/+}, Fig. 1A).

We confirmed the expression of *Wld^S* transcripts in retinas of suspect *Wld^S*^{+/+}, *Wld^S*^{+/-}, and C57 WT mice following the protocol described by [27]. Briefly, we euthanized mice by cervical dislocation and quickly removed retinas. We then extracted total RNA based on manufacturer’s protocol (SV Total RNA Isolation System, Promega, Madison, WI). Next, we determined RNA concentration and purity (NanoDrop 8000, Thermo

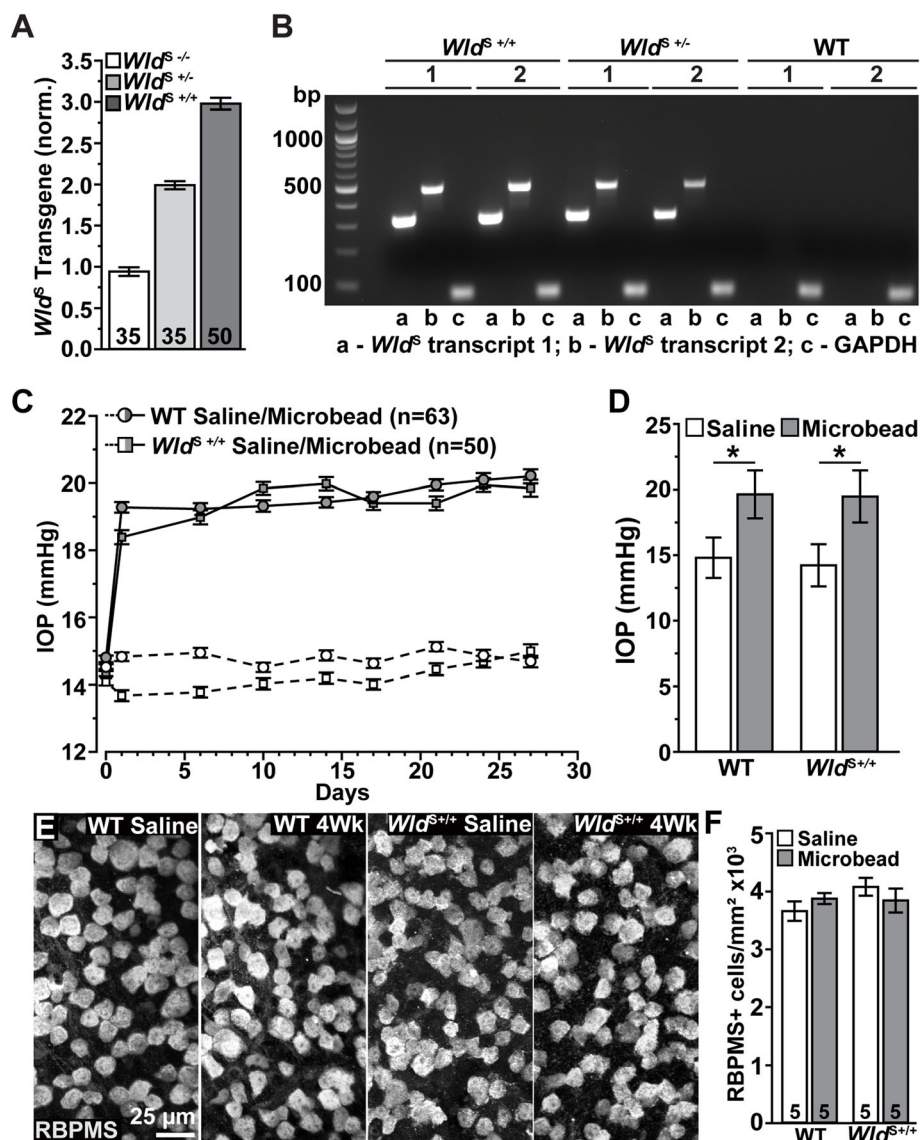


Fig. 1 Genotype Confirmation, IOP Elevation, and RGC Density Measurements. **A** Quantitative RT-PCR measurements of *Wld^S* transgene in genomic DNA from *Wld^S* null (*Wld^S*^{-/-}), *Wld^S* heterozygous (*Wld^S*^{+/-}), and *Wld^S* homozygous (*Wld^S*^{+/+}) mice. Values are normalized against WT animals. **B** Agarose gel (2%) showing RT-PCR detection in the retina of *Wld^S* chimeric (**a,b**) and housekeeping GAPDH (**c**) transcripts from *Wld^S*^{+/+}, *Wld^S*^{+/-}, and WT mice. 1,2 indicates samples extracted from different mice. **C** Mean intraocular pressure (IOP) in WT (circles) and *Wld^S*^{+/+} (squares) mice before (day 0) and following (days ≥ 1) a single unilateral injection of polystyrene microbeads (gray symbols) or equivalent volume of saline (white symbols). **D** Microbead injection significantly elevated IOP in all genotypes (WT: 19.64 \pm 1.82 vs. 14.81 \pm 1.54 mmHg, $p < 0.001$; *Wld^S*^{+/+}: 19.48 \pm 1.98 vs. 14.23 \pm 1.61 mmHg, $p < 0.001$). **E** Representative confocal images of whole-mount retinas from WT and *Wld^S*^{+/+} saline and microbead injected eyes immunolabeled against RBPMS (grayscale). Scale bar = 25 μ m. **F** When quantified, we did not detect a significant difference in RBPMS+ RGCs regardless of genotype or IOP condition ($p = 0.389$). Statistics: Student’s *t*-test (**D**). One-Way ANOVA Tukey’s Post hoc (**F**). Data = mean \pm SEM

Scientific, Wilmington, DE). Afterward, we reverse-transcribed mRNA into cDNA (1st Strand cDNA Synthesis System, Origene, Rockville, MD) and amplified the cDNA (QuantStudio 3 Real Time PCR System, Applied Biosystems, Waltham, MA) using the PowerUp SYBR Green Master Mix (Applied Biosystem, Waltham, MA) and the following primers: *Wld^S* transcript 1: forward (PE9): 5'-CAC GAC TTG CTG GTG GAC AGA-3' and reverse (PE4) 5'-GTC CTTGGC CAG CTC GAA CA-3'; *Wld^S* transcript 2: forward (PE9): 5' CAC GAC TTG CTG GTG GAC AGA-3' and reverse (PE6) 5'-TTT CCC ACG TAT CCA CTT CCA-3'. We used GAPDH as housekeeping gene; forward: 5'-TCC ATG ACA ACT TTG GCA TTG-3' and reverse 5'-CAG TCT TCT GGG TGG CAG TGA-3'. *Wld^S* transcripts were distinguished by electrophoresis of the RT-PCR product (2% agarose, 2% EtBr) and confirmed (ChemiDoc MP Imaging System, Bio-Rad, Hercules, CA, Fig. 1B).

Intraocular pressure elevation

Prior to intraocular pressure (IOP) elevation, baseline IOP was measured on 2 separate days by rebound tonometry (Tono-Pen XL; Medtronic Solan, Waltham MA) in anesthetized (2.5% isoflurane) mice. IOP was elevated in anesthetized (2.5% isoflurane) mice by a single unilateral injection of 1.5 μ L polystyrene microbeads (15 μ m, Invitrogen, Carlsbad CA) into the anterior chamber. We injected sterile phosphate buffered saline (PBS) into the contralateral eye to serve as an internal control. We measured IOP in anesthetized (2.5% isoflurane) mice bi-weekly [14, 29, 40–43]. For all mice used in this study, a single microbead injection increased IOP ~ 30% compared to saline-injected eyes, and IOP remained elevated for the duration (4 weeks, Fig. 1C, D).

Retinal ganglion cell physiology

Mice were euthanized by cervical dislocation, and whole retinas were removed under long-wavelength illumination (630 nm, 800 μ W/cm², FND/FG, Ushio, Cypress, CA). To aid in the removal of vitreous membrane from the retinal surface, we incubated retinas in a solution containing collagenase (LS005273, Worthington Biochemical, Lakewood, NJ), hyaluronidase (LS002592, Worthington Biochemical, Lakewood, NJ), and carbogen-saturated Ames' medium (US Biologic, Memphis, TN) for 10 mins on a rocker as described by [44]. Afterwards, retinas were rinsed within fresh Ames' medium and placed into physiological chamber mounted on an upright microscope (BX50, Olympus, Center Valley, PA). Retinas were maintained in the dark at 32 °C (TC-344B; Warner Instruments), and constantly perfused (2 mL/min) with carbogen-saturated NaHCO₃-buffered (22.6 mM) Ames' medium plus 20 mM glucose (Osm 290, pH 7.4). For RGC intracellular filling and patch-clamp recordings, we used fire-polished borosilicate glass pipettes

containing (in mM) 125 K-gluconate, 10 KCl, 10 HEPES, 10 EGTA, 4 Mg-ATP, 1 Na-GTP, and 0.1 ALEXA 555 (Invitrogen, Carlsbad CA; Osm 285, pH 7.35). RGC light responses were evoked using full-field light flashes generated by a light-emitting diode (365 nm, 300 μ W/cm², 3-s duration; Roithner Lasertechnik) delivered through a shutter in the microscope condenser [29, 34].

Retinal immunohistochemistry and imaging

After electrophysiological recordings, we fixed retinas overnight in 4% paraformaldehyde and immunolabeled them with the following primary antibodies: non-phosphorylated neurofilament H (SMI-32, 1:1000; BioLegend, San Diego, CA), choline acetyltransferase (ChAT, AB144P, 1:100, Millipore, Burlington, MA), and s-opsin (abn1660, 1:500, Millipore). In a subset of experiments, we immunolabeled whole-mount retinas against RNA-binding protein with multiple splicing (RBPMS, GTX118619, GeneTex, Irving, CA). Retinas were incubated with appropriate secondary antibodies (1:200; Jackson ImmunoResearch Laboratories, Inc., West Grove, PA) and mounted with Fluoromount G (Southern Biotech, Birmingham, AL). We imaged retinas using an Olympus FV-1000 inverted confocal microscope. We measured the density of RBPMS-positive RGCs by capturing four 0.0448 mm² images from whole-mounted retinas along the midline of each retinal quadrant. After imaging, we counted the number of cells positive for RBPMS, and we calculated RGC density as RGCs/mm².

Retinal ganglion cell dendritic morphology analysis

After imaging, micrographs of RGCs dendritic arbors were montaged and manually traced using Adobe Illustrator and Adobe Photoshop, respectively. We analyzed the skeletonized arbors by measuring the following parameters: dendritic field area, total dendritic length, dendritic intersections, and branch points. Dendritic field area was defined by outlining the distal dendritic tips and calculating the area of the resultant polygon. Total dendritic length was defined as the summation of all dendrites. The number of dendritic intersections was determined by Sholl analysis (ImageJ, 1.53c). Dendritic branch points were analyzed manually by counting the number of dendritic bifurcations [34].

Anterograde axonal transport

We anesthetized mice with 2.5% isoflurane and injected 1.5 μ L of 1 μ g/ μ L solution of cholera toxin subunit B (CTB) conjugated to Alexa Fluor 488 (Molecular Probes, Eugene, OR) into the vitreous of both eyes. Forty-eight hours later we perfused mice transcardially with PBS followed by 4% paraformaldehyde. Brains were removed and cryoprotected in 20% sucrose and coronal midbrain sections (50 μ m) cut on a freezing sliding microtome.

We imaged alternating sections of the superior colliculus (SC) using a Nikon Ti Eclipse microscope (Nikon Instruments Inc., Melville, NY) and quantified the intensity of CTB signal (intact transport) using a custom ImagePro macro (Media Cybernetics, Bethesda, MD) as previously described [4]. We confirmed CTB uptake by RGCs in the retinas using an Olympus FV-1000 inverted confocal microscope.

Behavioral spatial acuity

We placed unrestrained mice on an elevated platform located in the center of an arena surrounded by four adjoining computer monitors (OptoMotry; Cerebral Mechanics Inc., Canada [45]). We measured spatial frequency thresholds by assessing the optomotor response to drifting sinusoidal gratings at 100% contrast. Grating spatial frequency was systematically adjusted based on the optomotor response noted by naïve experimenters. Mice were tested 3 times before microbead injection (baseline) and twice a week for 4 weeks after injection [29, 43]. We analyzed spatial acuity data by calculating the difference in spatial acuity (Δ spatial acuity) of microbead and saline injected eyes.

Statistical analysis

All data are presented as mean \pm standard error of the mean (SEM). Statistics were performed using Graphpad 8.0 (Graphpad Software, San Diego, CA). We first assessed data for outliers using Grubb's test. Then, we determined whether data best fit normal or lognormal distributions. We used the Shapiro-Wilk test for normality. If data best fit a lognormal distribution, datasets were transformed by computing the logarithm (base 10) [34, 46]. For normal or transformed data, we performed parametric statistics. If datasets fit undetermined distributions or mix distributions (normal and lognormal), we performed non-parametric statistics. Statistical significance was defined as $p \leq 0.05$.

Results

Neuroprotection by *Wld^S* is dependent on RGC type during glaucoma

We verified the genotype of each *Wld^S* mouse by measuring the number of transgene copies relative to C57Bl/6 (WT) mice. These formed a continuum ranging from null (*Wld^{S-/-}*, corresponding to WT) to 2.5 and above (Fig. 1A), which we defined as *Wld^{S+/+}* following previous studies [27, 38]. For a subset of mice, we compared *Wld^{S+/+}*, *Wld^{S+/-}*, and WT designation in whole retina by probing for both *Wld^S* transcripts (318 bp and 478 bp) compared to GAPDH (71 bp; Fig. 1B). While naïve intraocular pressure (IOP) did not differ between WT left and right eyes nor between *Wld^{S+/+}* left and right eyes ($p \geq 0.17$), we detected a modest difference in IOP

between WT and *Wld^{S+/+}* naïve eyes (14.64 ± 0.13 vs. 14.1 ± 0.13 mmHg, respectively, $p = 0.006$). This small difference persisted in eyes receiving a saline injection as internal control (Fig. 1C) but was not significant when averaged over the one-month experimental period ($p = 0.79$, Fig. 1D). In contrast, an injection of microbeads into the anterior chamber following our established protocol elevated IOP in both WT (+ 32.6%, 19.64 ± 1.82 vs. 14.81 ± 1.5 mmHg) and *Wld^{S+/+}* (+ 36.8%, 19.48 ± 1.97 vs. 14.23 ± 1.61 mmHg) compared to saline-injected eyes ($p < 0.001$, Fig. 1D). Next, we determined if genotype or IOP elevation influenced RGC density by immunolabeling whole-mount retinas against RNA-binding protein with multiple splicing (RBPMS, [47], Fig. 1E). When quantified, we did not detect a significant difference in RBPMS+ RGCs regardless of genotype or IOP condition (WT saline: 3662.15 ± 142.12 , WT microbead 3879.73 ± 155.85 , *Wld^{S+/+}* saline: 4083.55 ± 154.86 , *Wld^{S+/+}* microbead: 3845.82 ± 207.12 RBPMS+ RGCs/mm², $p = 0.389$, Fig. 1F).

We targeted α -Sustained RGCs of the same type between WT and *Wld^{S+/+}* retinas based on large cell body, dendritic stratification within the inner plexiform layer (IPL), immunoreactivity for non-phosphorylated neurofilament H (SMI-32), and response to light following previous work [29, 32–34, 48]. Both WT and *Wld^{S+/+}* α ON-sustained (α ON-S) RGCs expressed SMI-32, with dendrites ramifying proximal to choline acetyltransferase (ChAT)-positive amacrine cell processes defining the "ON" sublamina of the IPL (Fig. 2A). These cells maintained a low spontaneous firing rate in darkness and produced a robust sustained train of action potentials in response to light, which appeared more robust for *Wld^{S+/+}* α ON-S RGCs (Fig. 2B). When quantified, we found *Wld^{S+/+}* α ON-S RGCs produced significantly greater responses to light as measured by the mean response (+ 68%, $p < 0.001$), the integrated response (+ 53%, $p = 0.008$), and the peak response to light compared to WT counterparts (+ 50%, $p < 0.001$; Fig. 2C). Even so, the resting membrane potential (RMP) of WT and *Wld^{S+/+}* control α ON-S RGCs was similar ($p = 0.47$, Fig. 2D), suggesting these differences were not due to a higher degree of resting depolarization. When quantified by Sholl analysis, the dendritic morphology of WT and *Wld^{S+/+}* control α ON-S RGCs were similar ($p \geq 0.52$) as were the number of branch points ($p = 0.23$), field area ($p = 0.79$), and total dendrite length ($p = 0.89$; Fig. 2E, F). However, α ON-S RGC somas from *Wld^{S+/+}* control retinas were significantly larger than WT counterparts (+ 17%, $p = 0.01$, Fig. 2F).

Previously we found that 1 month of IOP elevation reduces both dendritic complexity and RGC light responses, while 2 weeks enhances RGC excitability [29, 34]. Consistent with these results, 1 month of IOP elevation significantly decreased dendritic complexity of WT

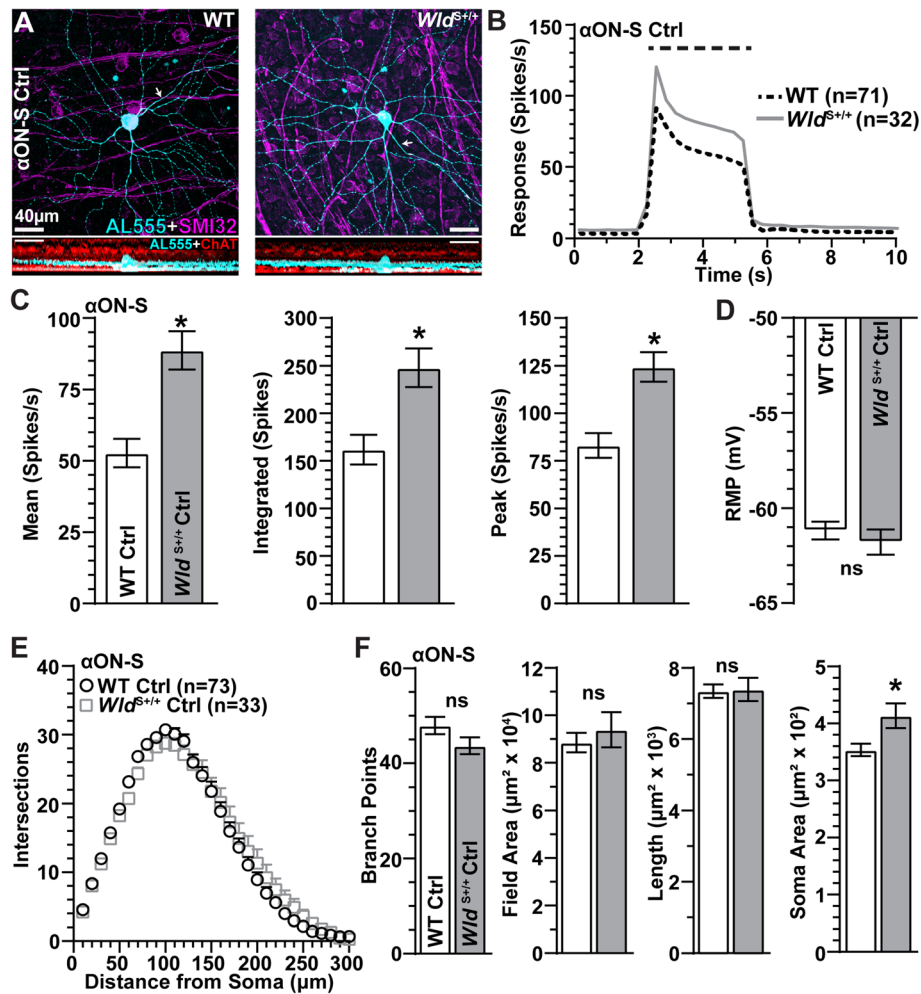


Fig. 2 Morphological and Physiological Characterization of α ON-Sustained RGCs in WT and *Wld^{S+/+}* Control Retinas. **A** Example *en face* (top) and orthogonal (bottom) images of dye-filled (AL555, cyan) α ON-S RGCs from WT and *Wld^{S+/+}* Ctrl animals. α ON-S RGCs were identified by positive immunolabeling against SMI-32 (magenta) and dendritic projections within the ON sublamina of the IPL identified by ChAT (red) immunolabeling. **B** Average light-evoked (3 s 365 nm, horizontal dashed line) spike rate histograms (300 ms bin width) of α ON-S RGCs from WT and *Wld^{S+/+}* Ctrl eyes. **C** *Wld^{S+/+}* Ctrl α ON-S RGC light responses are more robust than WT's (*, $p \leq 0.008$), **D** but RMP of WT and *Wld^{S+/+}* Ctrl α ON-S RGCs is similar ($p = 0.47$). **E** Sholl analysis of WT and *Wld^{S+/+}* Ctrl α ON-S RGCs. **F** Dendritic branch points, field area, and length are similar between WT and *Wld^{S+/+}* Ctrl α ON-S RGCs ($p \geq 0.23$), but *Wld^{S+/+}* somas are significantly larger ($p = 0.01$). WT Ctrl group contained cells from WT saline ($n = 59$) and WT naive ($n = 14$) eyes. *Wld^{S+/+}* Ctrl group consisted of cells from *Wld^{S+/+}* saline-injected ($n = 18$) and naive ($n = 15$) eyes. Statistics: Mann-Whitney tests (C, D, F, Field Area, Soma Size); Two-Way Repeated Measures ANOVA, Bonferroni post hoc tests (E), Student's *t*-tests (F, branch points and length). Scale bars = 40 μm . Arrows indicate RGC axons. Data = mean \pm SEM

α ON-S cells as measured by Sholl analysis ($p \leq 0.05$, Fig. 3A, B). The number of dendritic branch points also significantly decreased (-24% , $p < 0.001$), while dendritic field area and cross-sectional soma area did not change ($p \geq 0.14$, Fig. 3C). In contrast, elevated IOP had little discernable effect on the complexity of α ON-S RGCs from *Wld^{S+/+}* retina compared to control, again as measured by Sholl analysis ($p \geq 0.37$; Fig. 3D, E). Similarly, *Wld^{S+/+}* protected dendritic branch points ($p = 0.51$), field area ($p = 0.30$), and soma area ($p = 0.79$, Fig. 3F).

As before [29], a month of elevated IOP reduced the response of α ON-S RGCs from WT control

retinas (Fig. 4A), including the mean (-23%), peak (-30%), and integrated (-31%) response to light ($p \leq 0.002$, Fig. 4B). The RMP was more depolarized ($+5\%$) as well ($p = 0.001$, Fig. 4C). In contrast IOP did not influence the response of *Wld^{S+/+}* α ON-S RGCs (Fig. 4D), as the mean, peak, and integrated response did not change relative to control ($p \geq 0.55$, Fig. 4E). Unlike WT α ON-S RGCs, RMP did not change with IOP elevation ($p = 0.24$, Fig. 4F). Thus, *Wld^{S+/+}* protects α ON-S RGCs against stress-induced pruning of dendritic arbors and reductions in response that would ensue.

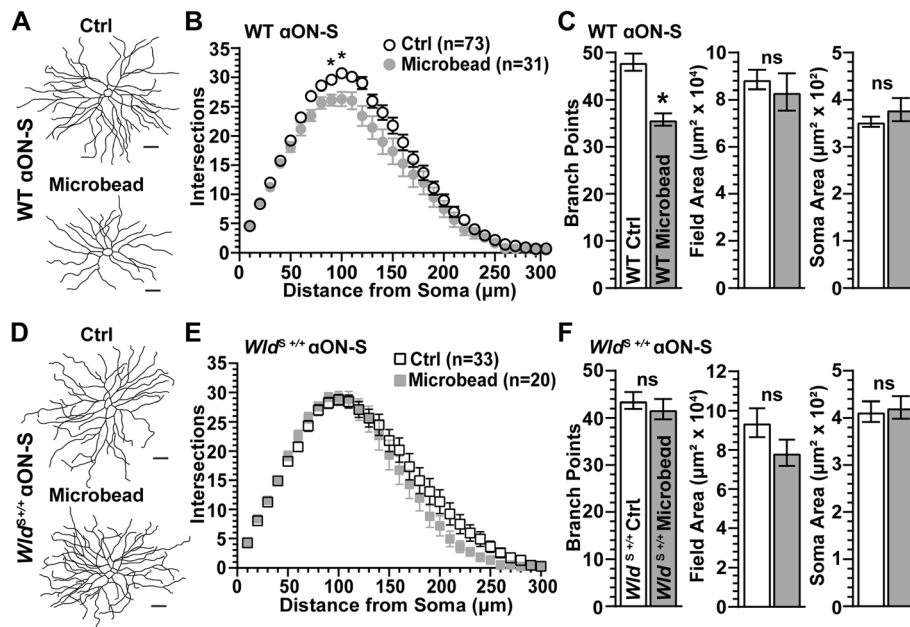


Fig. 3 *Wld^{S+/+}* Prevents Dendritic Pruning of α ON-S RGCs During IOP Elevation. **A** Reconstructed dendritic arbors of WT α ON-S RGCs from Ctrl and microbead-injected eyes. **B** Sholl analysis shows IOP elevation reduced the number of dendritic intersections between 90 and 100 μ m from soma ($p \leq 0.05$) of WT α ON-S RGCs. **C** Similarly, IOP elevation significantly decreased the number of branching points in WT α ON-S RGC dendrites ($p < 0.001$). For WT α ON-S RGCs, IOP elevation did not significantly affect dendritic field area ($p = 0.14$) or soma area ($p = 0.25$). **D** Reconstructed dendritic arbors of *Wld^{S+/+}* α ON-S RGCs from Ctrl and microbead-injected eyes. **E** Sholl analysis shows IOP elevation does not significantly affect the number of dendritic crossings in *Wld^{S+/+}* α ON-S RGC ($p \geq 0.37$). **F** Dendritic branching ($p = 0.51$), field area ($p = 0.30$), and soma area ($p = 0.79$) of *Wld^{S+/+}* α ON-S RGCs remain intact during IOP elevation. Statistics: Two-way repeated measures ANOVA, Bonferroni post hoc (**B, E**); Student's *t*-test (**C, F**). Scale bars = 50 μ m. Data presented as mean \pm SEM

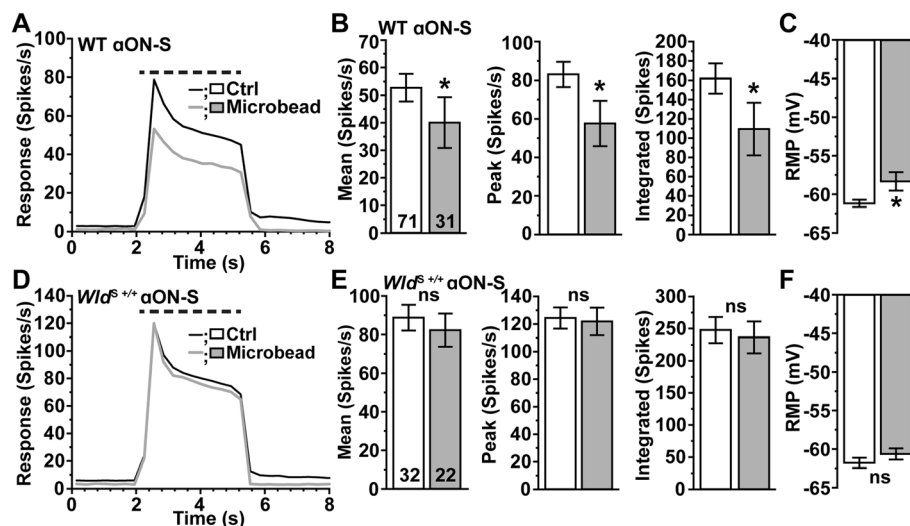


Fig. 4 *Wld^{S+/+}* Protects α ON-S RGC Light Responses and RMP During Glaucoma. **A** Mean light-evoked spike rate histograms (300 ms bin width) of α ON-S RGCs from Ctrl and microbead eyes of WT mice. **B** IOP elevation reduced light-evoked average spike rate ($-23\% 40.8 \pm 9$ vs. 52.7 ± 5 spikes/s, $p = 0.002$), peak spike rate (-30% , 58.3 ± 11.5 vs. 83.1 ± 6.5 spikes/s, $p = 0.0003$), integrated response (-31% , 111.7 ± 26.5 vs. 162 ± 15.6 spikes, $p = 0.0001$), and **C** depolarized RMP (-58.3 ± 1.2 vs. -61.2 ± 0.5 mV, $p = 0.02$). **D** Mean light-driven spike rate histograms of α ON-S RGCs from *Wld^{S+/+}* Ctrl and microbead eyes. **E** IOP elevation does not affect light-evoked mean firing rate ($p = 0.55$), peak spike rate ($p = 0.84$), integrated response ($p = 0.72$), or **F** RMP ($p = 0.24$) of *Wld^{S+/+}* α ON-S RGCs. Statistics: Mann-Whitney test (**B, C, F**); Student's *t*-test (**E**). Data = mean \pm SEM

Next, we examined the influence of *Wld^{S+/+}* on the morphology and physiology of α OFF-S RGCs with IOP elevation. Following previous work, we identified α OFF-S RGCs in WT and *Wld^{S+/+}* retinas based on dendritic projections within the IPL, immunoreactivity to SMI-32, and their responses to light [29, 32–34]. In WT and *Wld^{S+/+}* retinas, α OFF-S RGCs modestly express SMI-32 and have large somas with large, complex dendritic fields that project within the distal OFF sublamina of the IPL near ChAT-positive amacrine cell processes (Fig. 5A). These RGCs produced a high rate of spontaneous activity in darkness, which was inhibited by light onset, and

generated a sustained train of action potentials following light offset (Fig. 5B). Like *Wld^{S+/+}* α ON-S RGCs (Fig. 2B), the analogous response of *Wld^{S+/+}* α OFF-S RGCs was more robust than WT (Fig. 5B), with a significantly higher peak response (+ 28%, $p = 0.03$; Fig. 5C). As with α ON-S RGCs, *Wld^{S+/+}* did not affect the RMP of α OFF-S cells ($p = 0.17$, Fig. 5D). Unlike α ON-S RGCs, *Wld^{S+/+}* moderately reduced dendritic complexity of α OFF-S RGCs, with significantly less dendritic branch points (– 19%, $p = 0.005$, Fig. 5E, F). However, dendritic field area, total dendrite length, and soma area did not differ compared to WT ($p \geq 0.14$, Fig. 5F).

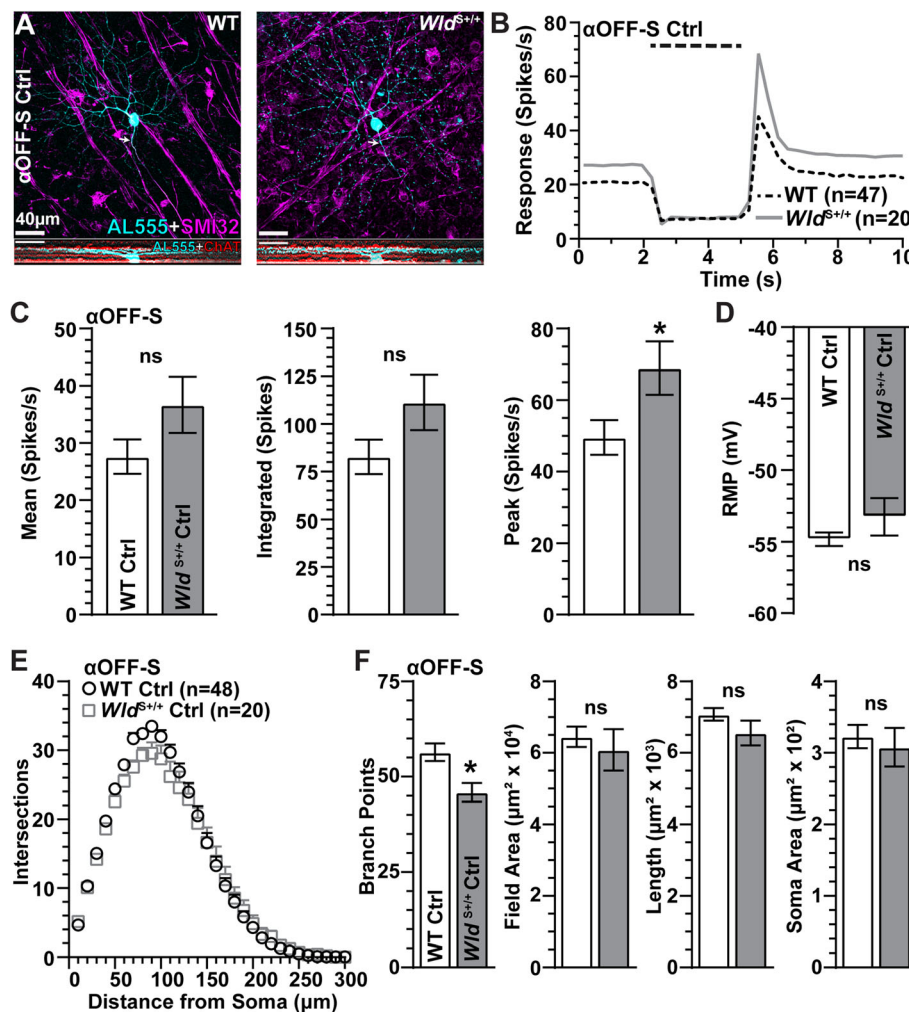


Fig. 5 Morphological and Physiological Comparison of α OFF-Sustained RGCs from WT and *Wld^{S+/+}* Control Retinas. **A** Representative forward (top) and orthogonal (bottom) projection micrographs of dye-filled (AL555, cyan) α OFF-S RGCs from Ctrl eyes of WT and *Wld^{S+/+}* animals. α OFF-S RGCs were identified by modest immunolabeling against SMI-32 (magenta) and dendritic projections within the distal OFF sublamina of the IPL identified by ChAT (red) immunoreactivity. **B** Mean light-driven spike rate histograms of α OFF-S RGCs from WT and *Wld^{S+/+}* retinas from Ctrl eyes. **C** α OFF-S RGC light-evoked mean ($p = 0.08$), integrated ($p = 0.07$), and peak ($p = 0.03$) responses are enhanced by *Wld^{S+/+}* versus WT Ctrl cells. **D** RMP is similar for WT and *Wld^{S+/+}* Ctrl α OFF-S RGCs ($p = 0.17$). **E** Sholl analysis of WT and *Wld^{S+/+}* Ctrl α OFF-S RGC dendrites ($p \geq 0.09$). **F** The average number of dendritic branch points of α OFF-S RGCs is reduced by *Wld^{S+/+}* ($p = 0.005$), but dendritic field area ($p = 0.52$), dendritic length ($p = 0.14$), and soma area ($p = 0.50$) are similar to WTs. WT Ctrl group consisted of cells from WT saline ($n = 38$) and WT naïve ($n = 10$) eyes. *Wld^{S+/+}* Ctrl group contained cells from *Wld^{S+/+}* saline-injected ($n = 12$) and naïve ($n = 8$) eyes. Statistics: Mann-Whitney test (**C**); Student's *t*-test (**D**, **F**); Two-Way Repeated Measures ANOVA, Bonferroni post hoc tests (**E**). Scale bars = 40 μ m. Data are expressed as mean \pm SEM

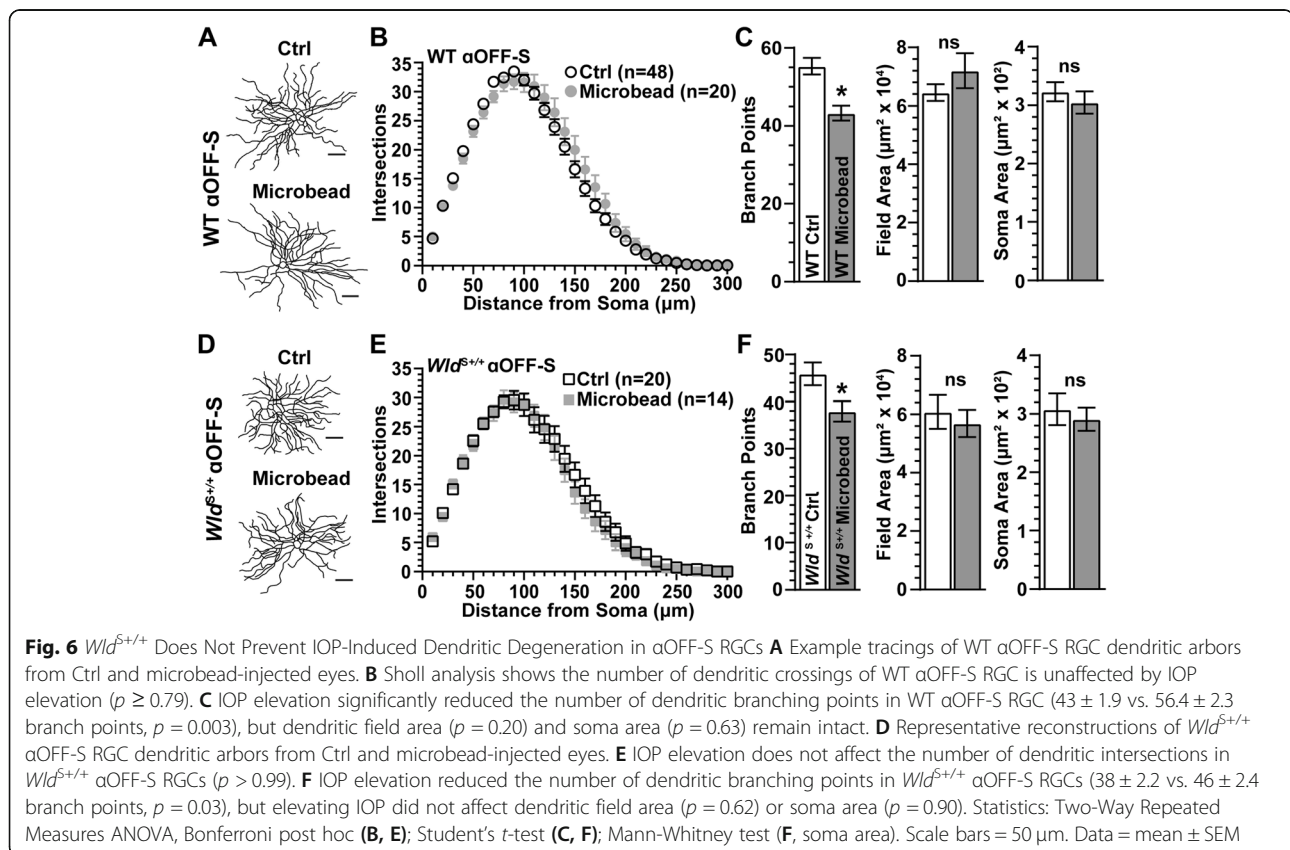
Based on Sholl analysis, a month of IOP elevation did not influence the number of dendritic intersections of WT α OFF-S RGCs ($p \geq 0.79$, Fig. 6B). Even so, the number of branch points in these cells reduced by 23% compared to control cells ($p = 0.003$), even as dendritic field area and cross-sectional soma area did not change ($p \geq 0.20$, Fig. 6C). Similarly, IOP elevation did not appear to alter dendritic morphology of $Wld^{S+/+}$ α OFF-S RGCs (Fig. 6D). Based on Sholl analysis, IOP elevation did not significantly affect the number of dendritic crossings ($p > 0.99$). However, as with WT, $Wld^{S+/+}$ α OFF-S RGCs demonstrated reduced branch points (-17% , $p = 0.03$), but no change in dendritic field area or soma area ($p \geq 0.62$; Fig. 6E, F). Thus, unlike α ON-S RGCs (Fig. 3D-F), $Wld^{S+/+}$ does not prevent loss of dendritic branch points in α OFF-S RGCs following IOP elevation.

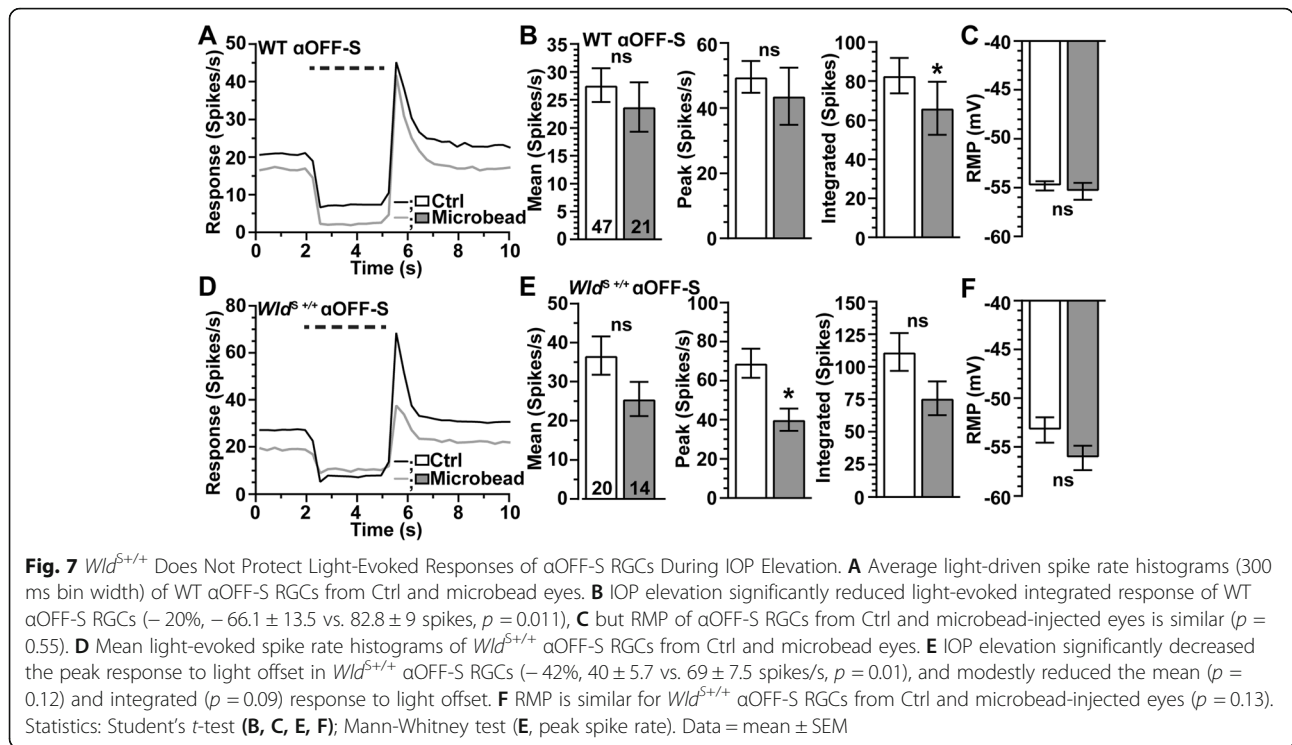
With a month of elevated IOP, α OFF-S RGCs in WT retina demonstrated less overall activity before, during and after light presentation (Fig. 7A), consistent with our previous work [29]. As before, the integrated response to light offset reduced significantly (-20% , $p = 0.011$), while the mean and peak response to offset did not change ($p \geq 0.12$, Fig. 7B). The RMP did not change with elevated IOP, in contrast to the more depolarized RMP of WT α ON-S RGCs ($p = 0.55$, Fig. 4C). In contrast to α ON-S RGCs, elevated IOP decreased the light

response of α OFF-S RGCs from $Wld^{S+/+}$ retinas (Fig. 7D), reducing the peak firing rate by 42% ($p = 0.01$, Fig. 7E). Thus, $Wld^{S+/+}$ is insufficient for the protection of mechanisms driving light-evoked responses of α OFF-S RGCs following a month of IOP elevation Table 1.

Age-dependent influence of $Wld^{S+/+}$ on axon transport and spatial acuity

The protective capacity of Wld^S depends on age, even though Wld^S expression does not change with age [20, 49, 50]. Here, we tested how aging impacts $Wld^{S+/+}$ protection of anterograde axon transport to the superior colliculus (SC) and spatial frequency threshold (i.e., spatial acuity) in the context of glaucoma. We first established a basis for testing the influence of aging on $Wld^{S+/+}$ protective capacity in young mice (aged 6–8 weeks). A month of IOP elevation significantly degraded anterograde transport of cholera toxin subunit B (CTB) to the SC in WT mice (Fig. 8A), while transport from $Wld^{S+/+}$ eyes remained largely intact (Fig. 8B). When quantified, elevated IOP reduced the percentage of intact transport to the SC by 36% compared to control in WT animals ($p < 0.001$, Fig. 8C), a significant difference compared to $Wld^{S+/+}$ ($p = 0.007$, Fig. 8C). For WT mice, spatial acuity significantly diminished over the experimental period ($R^2 = 0.80$, $p = 0.002$), while acuity for





Wld^{S+/+} did not change ($R^2 = 0.18$, $p = 0.28$) and remained better than WT over the course of IOP elevation ($p \leq 0.05$, Fig. 8D). Our results indicate *Wld^{S+/+}* prevents significant loss of axon transport and spatial acuity following 1 month of IOP elevation in young mice.

Next, we tested the influence of age on the protective capacity of *Wld^S* on anterograde axon transport and spatial acuity following IOP elevation. We again elevated IOP by unilateral microbead injection but using aged (1

year old) WT and *Wld^{S+/+}* animals (Fig. 9A). A single injection of microbeads similarly increased IOP in both WT (+29.6%, 19.45 ± 1.52 vs. 15.01 ± 1.28 mmHg) and *Wld^S* eyes (+29.76, 19.23 ± 1.67 vs. 14.82 ± 1.37 mmHg). Four weeks of IOP elevation reduced intact anterograde axon transport in aged WT mice slightly more than it did for young, 41% vs. 36% ($p = 0.74$; Fig. 9B, D). Interestingly, aged *Wld^{S+/+}* animals also demonstrated degraded transport with elevated IOP compared to control

Table 1 Descriptive Statistics for Dendritic Morphological and Physiological Measurements of αON- and αOFF-S RGCs from Control and Microbead Eyes of WT and *Wld^{S+/+}* Animals. Values are expressed as mean ± SEM

Genotype/ Cell Type	IOP Condition	Soma Area (μm^2)	Branch Points	Field Area (μm^2)	Length (μm)	Spike Rate (Mean)	Spike Rate (Peak)	Integrated Response (Spikes)	RMP (mV)
WT αON-S	Control	353±11	48±2	88594±4104	7348±191	58±5	83±6	162±16	-61±0.5
WT αON-S	Microbead	340±23	35±1	76922±7429	6887±194	41±9	58±11	112±26	-58±1.2
<i>Wld^{S+/+}</i> αON-S	Control	413±24	44±2	93942±7427	7395±328	89±7	124±8	248±20	-62±0.6
<i>Wld^{S+/+}</i> αON-S	Microbead	422±24	42±2	80177±6877	7017±381	82±9	122±10	236±26	-60.6±0.7
WT αOFF-S	Control	323±16	56±2	64510±2858	7080±176	28±3	50±5	83±9	-55±0.5
WT αOFF-S	Microbead	305±19	43±2	72025±5979	7373±393	23±4	44±9	66±13	-55±0.8
<i>Wld^{S+/+}</i> αOFF-S	Control	308±27	46±2	60848±5798	6558±345	37±5	68±7	111±15	-53±1.3
<i>Wld^{S+/+}</i> αOFF-S	Microbead	291±20	38±2	56880±4658	6412±298	25±4	40±6	76±13	-56±1.2

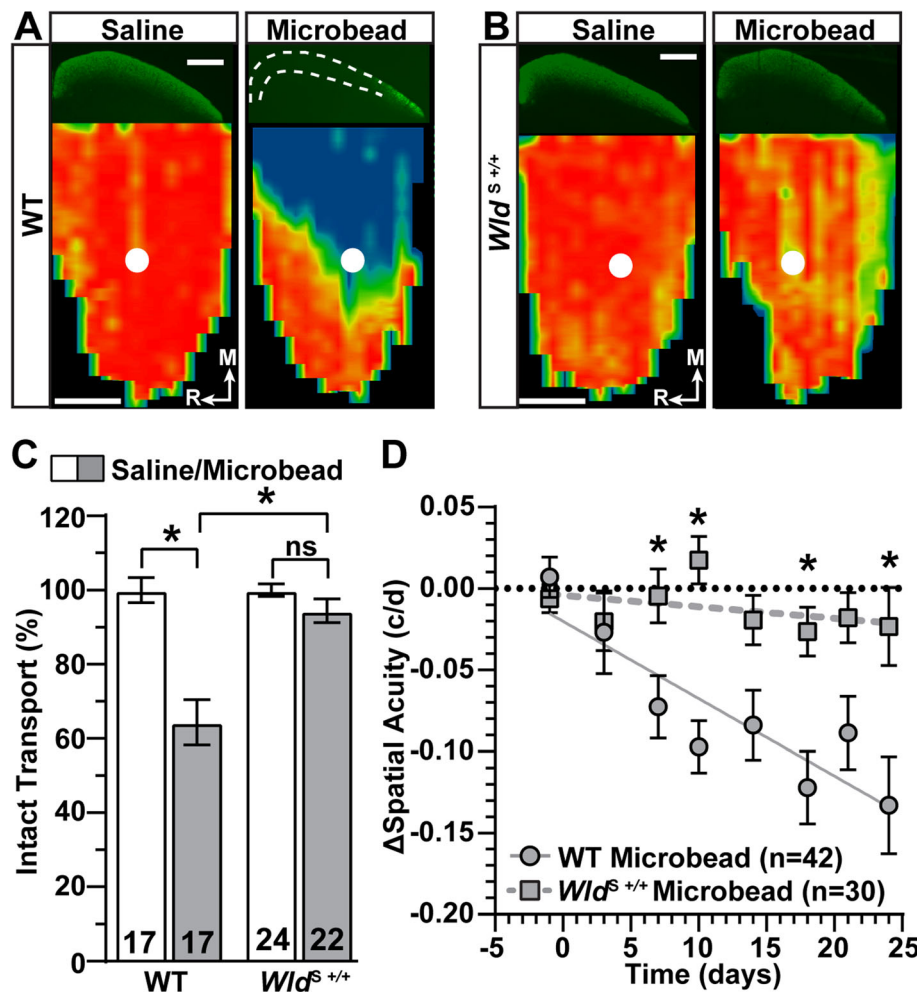


Fig. 8 *Wld^{S+/+}* Protects Anterograde Axon Transport and Spatial Acuity Following IOP Elevation in Young Mice. **A, B** Representative coronal sections (top) of the superior colliculus (SC) following intravitreal injection of CTB-488 (green) into saline- and microbead-injected eyes of WT (**A**) and *Wld^{S+/+}* (**B**) mice. Transport deficits indicated by dashed lines. Retinotopic maps (bottom) reconstructed from serial sections of SC with optic disc indicated (white circles). Density of the transported CTB signal ranges from 0% (blue) to 50% (green) to 100% (red). Medial (M) and rostral (R) orientations are indicated. Scale bar = 500 μ m. **C** Quantification of the intact anterograde transport (%) to the SC from saline- and microbead-injected eyes of WT and *Wld^{S+/+}* mice. IOP elevation significantly decreased transport in WT mice ($p < 0.001$) but transport is preserved in *Wld^{S+/+}* animals ($p > 0.99$) and significantly greater than WT microbead eyes ($p = 0.007$). **D** Difference in spatial acuity threshold (cycles/degree, c/d) between saline and microbead eyes (microbead-control, Δ) from WT and *Wld^{S+/+}* mice. Spatial acuity linearly diminishes over time in WT ($R^2 = 0.80$, $p = 0.002$) but remains stable in *Wld^{S+/+}* mice ($R^2 = 0.18$, $p = 0.283$). Δ spatial acuity is significantly greater in *Wld^{S+/+}* versus WT mice (*, $p \leq 0.05$). Statistics: Kruskal-Wallis test, Dunn’s post hoc (**C**), Linear mixed model (**D**), Linear regression (**D**). Data = mean \pm SEM

eyes (-15%; $p \leq 0.03$, Fig. 9C,D), though still retaining significantly more intact transport compared to either young or aged WT eyes challenged by elevated IOP ($p \leq 0.002$). Aging also influenced spatial acuity. Elevated IOP induced a decrease not only in WT ($p = 0.0064$), but also in *Wld^{S+/+}* animals ($p = 0.0058$, Fig. 9E), which significantly exceeded the rate of reduction in younger *Wld^{S+/+}* animals ($p < 0.001$). The rate of degradation in acuity was similar between aged WT and *Wld^{S+/+}* mice ($p = 0.35$). Thus, aging reduces the neuroprotective benefit of *Wld^{S+/+}* not only on axonal transport but also throughout the optic projection.

Discussion

Extent of neuroprotection by *Wld^S* is dependent on RGC type during glaucoma

Our first finding is neuroprotection by *Wld^{S+/+}* during glaucoma appears to depend on RGC type. Our results suggest *Wld^{S+/+}* confers neuroprotection in α ON-S RGCs but not α OFF-S RGCs. Following 1 month of IOP elevation by microbead occlusion, WT α ON-S RGC dendritic crossings (Sholl analysis) and branch points decreased while *Wld^{S+/+}* α ON-S RGC dendritic arbors remained intact (Fig. 3). This result suggests *Wld^{S+/+}* not only protects RGC somas and axons during glaucoma

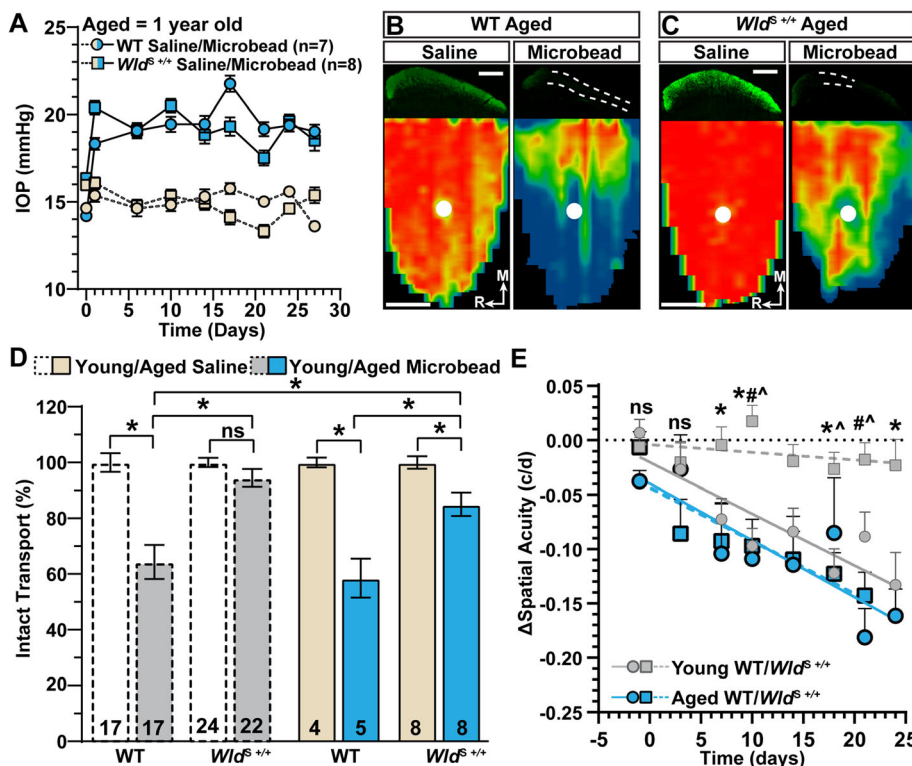


Fig. 9 Aging Reduces the Neuroprotective Capacity of *Wld^{S+/+}*. **A** IOP of aged WT (circles) and *Wld^{S+/+}* (squares) mice before (day 0) and after (days ≥ 1) a single unilateral injection of microbeads (blue symbols) or equivalent volume of saline (beige symbols). Microbeads elevated IOP by 29.5% in aged WT (19.45 ± 1.5 vs. 15.01 ± 1.3 mmHg, $p < 0.001$) and 29.7% in *Wld^{S+/+}* eyes compared to saline-injected eyes (19.23 ± 1.6 vs. 14.82 ± 1.3 mmHg, $p < 0.001$). **B, C** Example coronal sections (top) of the SC after intravitreal injection of CTB-488 (green) into saline- and microbead eyes of aged WT (**B**) and *Wld^{S+/+}* mice (**C**). Transport deficits are indicated by dashed lines. Retinotopic maps (bottom) recreated from SC sections with optic disc indicated by white filled circles. Scale bar = 500 μ m. **D** Quantification of anterograde axon transport to the SC. Data from young (1.5–2.5 months old) animals are replotted from Fig. 8C for comparison. We did not detect a difference in the percent of intact transport to the SCs corresponding to saline eyes of young vs. aged WT and *Wld^{S+/+}* animals ($p = 0.60$). For aged animals, IOP elevation decreased transport in WT ($p < 0.001$) and *Wld^{S+/+}* mice ($p = 0.03$) when compared to respective saline eyes. Axon transport of aged *Wld^{S+/+}* microbead-injected eyes was greater than that observed in SC of aged WT microbead eyes ($p = 0.001$). **E** Quantification of Δ spatial acuity. Data for young animals replotted from Fig. 8D for comparison. Spatial acuity linearly diminishes over the duration of IOP elevation in aged WT ($R^2 = 0.74$, $p = 0.0064$) and *Wld^{S+/+}* mice ($R^2 = 0.81$, $p = 0.0058$). Statistics: Student’s *t*-test (**A**), Kruskal-Wallis test, Dunn’s post hoc (**D**) Linear mixed model (**E**), Linear regression (**E**). Multiple comparison significance indicators: * Young WT vs. Young *Wld^{S+/+}*; # Aged WT vs. Young *Wld^{S+/+}*; \wedge Young *Wld^{S+/+}* vs. Aged *Wld^{S+/+}* (**E**). Data presented = mean \pm SEM

[22], but extends to dendrites of RGCs [25]. Regarding RGC physiology, we find 1 month of elevated IOP depolarizes RMP and reduces the mean, peak, and integrated response to light of WT α ON-S RGCs (Fig. 4A-C). While short term elevations in IOP increase RGC light responses and excitability, prolonged IOP elevation diminishes both [29, 51]. For *Wld^{S+/+}* α ON-S RGCs, RMP and light response properties are unaffected by IOP elevation (Fig. 4D-F). Our finding substantiates evidence that *Wld^{S+/+}* preserves the RGC pattern electroretinogram response during DBA2/J glaucoma [22]. Furthermore, our data suggests *Wld^{S+/+}* either indirectly or directly protects mechanisms that generate RMP and voltage-gated responses of α ON-S RGCs [29, 51].

Although *Wld^{S+/+}* provides extensive protection during glaucoma for dendritic arbors and mechanisms that

drive RMP and the light-evoked response of α ON-S RGCs, neuroprotection by *Wld^{S+/+}* is not robustly afforded to α OFF-S RGCs. We find IOP elevation significantly reduces the number of dendritic branch points of α OFF-S RGCs from WT and *Wld^{S+/+}* eyes (Fig. 6C, F). Moreover, we find 1 month of IOP elevation decreases the integrated light-evoked response of WT α OFF-S RGCs (Fig. 7B) and the peak response of *Wld^{S+/+}* α OFF-S RGCs (Fig. 7E).

Based on these data, *Wld^{S+/+}* appears to protect α ON-S RGCs but not α OFF-S cells. In support for this argument, evidence suggests OFF RGCs are more vulnerable to stress caused by IOP elevation [31–33]. Although this is a tantalizing conclusion, qualitative analysis reveals *Wld^S* protein is expressed in the nuclei of most cells in the RGC layer of *Wld^{S+/+}* mice, indicating RGCs should

be equally protected from stress by Wld^S [52]. However, the magnitude of neuroprotection following acute axonal injury is correlated with Wld^S expression levels in α - and γ -motor neuron neurons [53]. Thus, the possibility exists that Wld^S expression is dependent on RGC type.

The discrepancy between the extent of neuroprotection provided by Wld^S to α ON- and α OFF-S RGCs is further highlighted by the fact the duration of Wld^S neuroprotection is dependent on glaucoma model. Wld^S neuroprotection lasts months in chronic DBA2/J glaucoma but is restricted to 2–4 weeks following IOP elevation by photocoagulation of the trabecular meshwork [22, 52]. Therefore, it might be the case that both α ON- and α OFF-S RGC respond to Wld^S during stress, but the duration of protection by Wld^S is more transient for α OFF-S RGCs.

The duration of neuroprotection by Wld^S may be shorter for α OFF-S RGCs due to their intrinsic physiological properties. α OFF-S RGCs intrinsically generate greater spontaneous activity compared to α ON-S RGCs (Figs. 2 and 5B). Thus, α OFF-S RGCs may be more sensitive to stress due to the metabolic burden of persistent action potential generation and maintaining RMP. Cell excitability determines the magnitude of neuroprotection by Wld^S after nerve sectioning. “Enhancing axon excitability by high-frequency stimulation or blunting excitability by blocking voltage-gated sodium channels with tetrodotoxin both accelerate axon degeneration following axotomy of neuromuscular junctions in Wld^S mice” [54]. Considering these findings, α OFF-S RGCs may be more vulnerable to stress due to their intrinsically high spontaneous activity, which is further enhanced during early progression of glaucoma [29, 34].

Neuroprotective capacity of Wld^S is dependent on age during glaucoma

Our second key finding is neuroprotection by Wld^S on anterograde axonal transport and spatial acuity during glaucoma is dependent on age. As we have previously shown [29, 43], IOP elevation significantly reduces anterograde axonal transport and spatial acuity in young adult WT mice (Fig. 8). Both anterograde axon transport and spatial acuity are protected during glaucoma in young adult $Wld^{S+/+}$ mice (Fig. 8). Our data provide additional confirmatory evidence that $Wld^{S+/+}$ provides neuroprotection for axon transport during glaucoma [22–24]. Furthermore, our results indicate if axonopathy caused by IOP elevation is reduced, as is the case for young adult $Wld^{S+/+}$ animals (Fig. 8C), degradation of spatial acuity slows (Fig. 8D).

Although we find anterograde axonal transport and spatial acuity are preserved in young adult $Wld^{S+/+}$ animals, neuroprotection by Wld^S is reduced in aged, one-year old, animals following IOP elevation (Fig. 9). Even

so, Wld^S still offers some protection on anterograde axon transport in aged mice relative to age-matched WT mice (Fig. 9B–D). However, IOP elevation significantly reduces spatial acuity similarly for aged WT and $Wld^{S+/+}$ mice (Fig. 9E).

Our finding that neuroprotection by $Wld^{S+/+}$ depends on age is surprising because axon integrity and RGC pattern electroretinogram responses are preserved in 10 to 12 month old DBA2/J. Wld^S mice [22]. However, when the age range is narrowed to include only 12 month old DBA2/J. Wld^S mice, optic nerves possess more degenerating axons compared to age-matched DBA2/J. Wld^S mice supplemented with nicotinamide, indicating neuroprotection by Wld^S on axonopathy is reduced by advanced age in chronic DBA2/J. Wld^S glaucoma [24]. These data suggest neuroprotection by Wld^S falls off precipitously between 10 to 12 months of age in DBA2/J glaucoma. Following an inducible injury, the neuroprotective capacity of Wld^S is also age dependent, even though Wld^S expression levels do not change with age [20, 49, 50]. Taken together, the degree of neuroprotection by Wld^S appears to be highly sensitive to age, limiting the utility of targeting only Wld^S to block the progression of age-related neurodegenerative diseases [24, 55, 56].

Conclusions

We have demonstrated that $Wld^{S+/+}$ does not equally protect all RGC types even in young adult animals during glaucoma and neuroprotection by $Wld^{S+/+}$ on axonopathy is dependent on age. We find α OFF-S RGCs from $Wld^{S+/+}$ retinas are similarly susceptible to dendritic degeneration and degradation of RGC signaling during glaucoma as their WT counterparts. While $Wld^{S+/+}$ protects α ON-S RGC dendrites and light-evoked activity. The influence of $Wld^{S+/+}$ on anterograde axonal transport and spatial acuity is significantly blunted in aged animals. Although $Wld^{S+/+}$ confers significant neuroprotection of anterograde axon transport and spatial acuity during axonopathy in otherwise uncompromised systems, this protection is limited at the level of different RGC types and is age dependent.

Abbreviations

RGC: Retinal ganglion cells; Wld^S : Slow Wallerian degeneration; IOP: Intraocular pressure; WT: Wild type; RBPMS: RNA-binding protein with multiple splicing; RMP: Resting membrane potential; CTB: Cholera toxin subunit B; IPL: Inner plexiform layer; ChAT: Choline acetyltransferase; SC: Superior colliculus

Acknowledgements

We thank Dr. Shu-Wei Sun from Loma Linda University for donating the Wld^S mice.

Authors' contributions

M.L.R., S.P. and D.J.C. designed research; M.L.R., S.P., N.R.M., K.B.D., V.Y., M.L.C. performed research; M.L.R., S.P., N.R.M., and D.J.C. analyzed data; M.L.R., S.P., and D.J.C. wrote the paper. All authors read and approved the final manuscript.

Funding

Support provided by a departmental unrestricted award by the Research to Prevent Blindness Inc., Research to Prevent Blindness Inc. Stein Innovation Award, the Stanley Cohen Innovation Fund, and National Institutes of Health grants EY017427, EY024997, and EY008126 to DJC. Imaging supported through the Vanderbilt University Medical Center Cell Imaging Shared Resource core facility and NIH grants CA68485, DK20593, DK58404, and DK59637.

Availability of data and materials

The datasets used and/or analyzed during the current study are available from the corresponding author on reasonable request.

Declarations

Ethics approval and consent to participate

The Vanderbilt University Institutional Animal Care and Use Committee approved all experimental procedures described in this manuscript.

Consent for publication

All authors have approved the contents of this manuscript and provided consent for publication.

Competing interests

The authors declare that they have no competing interests.

Received: 5 February 2021 Accepted: 26 May 2021

Published online: 05 June 2021

References

- Coleman M. Axon degeneration mechanisms: commonality amid diversity. *Nat Rev Neurosci.* 2005;6(11):889–98. <https://doi.org/10.1038/nrn1788>.
- Morfini GA, Burns M, Binder LI, Kanaan NM, LaPointe N, Bosco DA, et al. Axonal transport defects in neurodegenerative diseases. *J Neurosci.* 2009;29(41):12776–86. <https://doi.org/10.1523/JNEUROSCI.3463-09.2009>.
- Saxena S, Caroni P. Mechanisms of axon degeneration: from development to disease. *Prog Neurobiol.* 2007;83(3):174–91. <https://doi.org/10.1016/j.pneurobio.2007.07.007>.
- Crish SD, Sappington RM, Inman DM, Horner PJ, Calkins DJ. Distal axonopathy with structural persistence in glaucomatous neurodegeneration. *Proc Natl Acad Sci U S A.* 2010;107(11):5196–201. <https://doi.org/10.1073/pnas.0913141107>.
- Calkins DJ. Critical pathogenic events underlying progression of neurodegeneration in glaucoma. *Prog Retin Eye Res.* 2012;31(6):702–19. <https://doi.org/10.1016/j.preteyeres.2012.07.001>.
- Tham YC, Li X, Wong TY, Quigley HA, Aung T, Cheng CY. Global prevalence of glaucoma and projections of glaucoma burden through 2040: a systematic review and meta-analysis. *Ophthalmology.* 2014;121(11):2081–90. <https://doi.org/10.1016/j.ophtha.2014.05.013>.
- Burgoyne CF. A biomechanical paradigm for axonal insult within the optic nerve head in aging and glaucoma. *Exp Eye Res.* 2011;93(2):120–32. <https://doi.org/10.1016/j.exer.2010.09.005>.
- Mafwiri M, Bowman RJ, Wood M, Kabiru J. Primary open-angle glaucoma presentation at a tertiary unit in Africa: intraocular pressure levels and visual status. *Ophthalmic Epidemiol.* 2005;12(5):299–302. <https://doi.org/10.1080/09286580500180572>.
- Leske MC, Heijl A, Hussein M, Bengtsson B, Hyman L, Komaroff E. Factors for glaucoma progression and the effect of treatment: the early manifest glaucoma trial. *Arch Ophthalmol.* 2003;121(1):48–56. <https://doi.org/10.1001/archophth.121.1.48>.
- Wareham LK, Risner ML, Calkins DJ. Protect, repair, and regenerate: towards restoring vision in Glaucoma. *Curr Ophthalmol Rep.* 2020;8(4):301–10. <https://doi.org/10.1007/s40135-020-00259-5>.
- Ferri A, Sanes JR, Coleman MP, Cunningham JM, Kato AC. Inhibiting axon degeneration and synapse loss attenuates apoptosis and disease progression in a mouse model of motoneuron disease. *Curr Biol.* 2003;13(8):669–73. [https://doi.org/10.1016/S0960-9822\(03\)00206-9](https://doi.org/10.1016/S0960-9822(03)00206-9).
- Her LS, Goldstein LS. Enhanced sensitivity of striatal neurons to axonal transport defects induced by mutant huntingtin. *J Neurosci.* 2008;28(50):13662–72. <https://doi.org/10.1523/JNEUROSCI.4144-08.2008>.
- Howell GR, Libby RT, John SW. Mouse genetic models: an ideal system for understanding glaucomatous neurodegeneration and neuroprotection. *Prog Brain Res.* 2008;173:303–21. [https://doi.org/10.1016/S0079-6123\(08\)01122-9](https://doi.org/10.1016/S0079-6123(08)01122-9).
- Calkins DJ, Lambert WS, Formichella CR, McLaughlin WM, Sappington RM. The microbead occlusion model of ocular hypertension in mice. *Methods Mol Biol.* 1695;2018:23–39.
- Dapper JD, Crish SD, Pang IH, Calkins DJ. Proximal inhibition of p38 MAPK stress signaling prevents distal axonopathy. *Neurobiol Dis.* 2013;59:26–37. <https://doi.org/10.1016/j.nbd.2013.07.001>.
- Lambert WS, Pasini S, Collyer JW, Formichella CR, Ghose P, Carlson BJ, et al. Of mice and monkeys: neuroprotective efficacy of the p38 inhibitor BIRB 796 depends on model duration in experimental Glaucoma. *Sci Rep.* 2020;10(1):8535. <https://doi.org/10.1038/s41598-020-65374-6>.
- Harder JM, Guymer C, Wood JPM, Daskalaki E, Chidlow G, Zhang C, et al. Disturbed glucose and pyruvate metabolism in glaucoma with neuroprotection by pyruvate or rapamycin. *Proc Natl Acad Sci U S A.* 2020;117(52):33619–27. <https://doi.org/10.1073/pnas.2014213117>.
- Coleman MP, Freeman MR. Wallerian degeneration, wld(s), and nmnat. *Annu Rev Neurosci.* 2010;33(1):245–67. <https://doi.org/10.1146/annurev-neuro-060909-153248>.
- Wright AK, Wishart TM, Ingham CA, Gillingwater TH. Synaptic protection in the brain of WldS mice occurs independently of age but is sensitive to gene-dose. *PLoS One.* 2010;5(11):e151108. <https://doi.org/10.1371/journal.pone.0015108>.
- Perry VH, Brown MC, Tsao JW. The effectiveness of the gene which slows the rate of Wallerian degeneration in C57BL/Ola mice declines with age. *Eur J Neurosci.* 1992;4(10):1000–2. <https://doi.org/10.1111/j.1460-9568.1992.tb00126.x>.
- Porciatti V, Saleh M, Nagaraju M. The pattern electroretinogram as a tool to monitor progressive retinal ganglion cell dysfunction in the DBA/2J mouse model of glaucoma. *Invest Ophthalmol Vis Sci.* 2007;48(2):745–51. <https://doi.org/10.1167/iov.06-0733>.
- Howell GR, Libby RT, Jakobs TC, Smith RS, Phalan FC, Barter JW, et al. Axons of retinal ganglion cells are insulted in the optic nerve early in DBA/2J glaucoma. *J Cell Biol.* 2007;179(7):1523–37. <https://doi.org/10.1083/jcb.200706181>.
- Howell GR, Soto I, Libby RT, John SW. Intrinsic axonal degeneration pathways are critical for glaucomatous damage. *Exp Neurol.* 2013;246:54–61. <https://doi.org/10.1016/j.expneurol.2012.01.014>. Epub 2012 Jan 18.
- Williams PA, Harder JM, Foxworth NE, Cardozo BH, Cochran KE, John SWM. Nicotinamide and WLD(S) act together to prevent neurodegeneration in Glaucoma. *Front Neurosci.* 2017;11:232. <https://doi.org/10.3389/fnins.2017.00232>.
- Harder JM, Braine CE, Williams PA, Zhu X, MacNicol KH, Sousa GL, et al. Early immune responses are independent of RGC dysfunction in glaucoma with complement component C3 being protective. *Proc Natl Acad Sci U S A.* 2017;114(19):E3839–e3848. <https://doi.org/10.1073/pnas.1608769114>.
- Coleman MP, Conforti L, Buckmaster EA, Tarlton A, Ewing RM, Brown MC, et al. An 85-kb tandem triplication in the slow Wallerian degeneration (Wlds) mouse. *Proc Natl Acad Sci U S A.* 1998;95(17):9985–90. <https://doi.org/10.1073/pnas.95.17.9985>.
- Conforti L, Tarlton A, Mack TG, Mi W, Buckmaster EA, Wagner D, et al. A Ufd2/D4Cole1e chimeric protein and overexpression of Rbp7 in the slow Wallerian degeneration (Wlds) mouse. *Proc Natl Acad Sci U S A.* 2000;97(21):11377–82. <https://doi.org/10.1073/pnas.97.21.11377>.
- Mack TG, Reiner M, Beirowski B, Mi W, Emanuelli M, Wagner D, et al. Wallerian degeneration of injured axons and synapses is delayed by a Ube4b/Nmnat chimeric gene. *Nat Neurosci.* 2001;4(12):1199–206. <https://doi.org/10.1038/nn770>.
- Risner ML, Pasini S, Cooper ML, Lambert WS, Calkins DJ. Axogenic mechanism enhances retinal ganglion cell excitability during early progression in glaucoma. *Proc Natl Acad Sci U S A.* 2018;115(10):E2393–e2402. <https://doi.org/10.1073/pnas.1714888115>.
- Chou TH, Romano GL, Amato R, Porciatti V. Nicotinamide-Rich Diet in DBA/2J Mice Preserves Retinal Ganglion Cell Metabolic Function as Assessed by PERG Adaptation to Flicker. *Nutrients.* 2020;12(7):1910. <https://doi.org/10.3390/nu12071910>.
- El-Danaf RN, Huberman AD. Characteristic patterns of dendritic remodeling in early-stage glaucoma: evidence from genetically identified retinal ganglion cell types. *J Neurosci.* 2015;35(6):2329–43. <https://doi.org/10.1523/JNEUROSCI.1419-14.2015>.

32. Della Santina L, Inman DM, Lupien CB, Horner PJ, Wong RO. Differential progression of structural and functional alterations in distinct retinal ganglion cell types in a mouse model of glaucoma. *J Neurosci*. 2013;33(44):17444–57. <https://doi.org/10.1523/JNEUROSCI.5461-12.2013>.
33. Ou Y, Jo RE, Ullian EM, Wong RO, Della Santina L. Selective vulnerability of specific retinal ganglion cell types and synapses after transient ocular hypertension. *J Neurosci*. 2016;36(35):9240–52. <https://doi.org/10.1523/JNEUROSCI.0940-16.2016>.
34. Risner ML, McGrady NR, Boal AM, Pasini S, Calkins DJ. TRPV1 supports Axogenic enhanced excitability in response to neurodegenerative stress. *Front Cell Neurosci*. 2020;14:603419.
35. Pang JJ, Gao F, Wu SM. Light-evoked excitatory and inhibitory synaptic inputs to ON and OFF alpha ganglion cells in the mouse retina. *J Neurosci*. 2003;23(14):6063–73. <https://doi.org/10.1523/JNEUROSCI.23-14-06063.2003>.
36. Krieger B, Qiao M, Rousoo DL, Sanes JR, Meister M. Four alpha ganglion cell types in mouse retina: function, structure, and molecular signatures. *PLoS One*. 2017;12(7):e0180091. <https://doi.org/10.1371/journal.pone.0180091>.
37. Sun SW, Nishioka C, Chung CF, Park J, Liang HF. Anterograde-propagation of axonal degeneration in the visual system of wlds mice characterized by diffusion tensor imaging. *J Magn Reson Imaging*. 2017;45(2):482–91. <https://doi.org/10.1002/jmri.25368>.
38. Wishart TM, Macdonald SH, Chen PE, Shipston MJ, Coleman MP, Gillingwater TH, et al. Design of a novel quantitative PCR (QPCR)-based protocol for genotyping mice carrying the neuroprotective Wallerian degeneration slow (Wlds) gene. *Mol Neurodegener*. 2007;2(1):21. <https://doi.org/10.1186/1750-1326-2-21>.
39. Schmittgen TD, Livak KJ. Analyzing real-time PCR data by the comparative C(T) method. *Nat Protoc*. 2008;3(6):1101–8. <https://doi.org/10.1038/nprot.2008.73>.
40. Sappington RM, Carlson BJ, Crish SD, Calkins DJ. The microbead occlusion model: a paradigm for induced ocular hypertension in rats and mice. *Invest Ophthalmol Vis Sci*. 2010;51(1):207–16. <https://doi.org/10.1167/iov.09-3947>.
41. Weitlauf C, Ward NJ, Lambert WS, Sidorova TN, Ho KW, Sappington RM, et al. Short-term increases in transient receptor potential vanilloid-1 mediate stress-induced enhancement of neuronal excitation. *J Neurosci*. 2014;34(46):15369–81. <https://doi.org/10.1523/JNEUROSCI.3424-14.2014>.
42. Ward NJ, Ho KW, Lambert WS, Weitlauf C, Calkins DJ. Absence of transient receptor potential vanilloid-1 accelerates stress-induced axonopathy in the optic projection. *J Neurosci*. 2014;34(9):3161–70. <https://doi.org/10.1523/JNEUROSCI.4089-13.2014>.
43. Cooper ML, Pasini S, Lambert WS, D'Alessandro KB, Yao V, Risner ML, et al. Redistribution of metabolic resources through astrocyte networks mitigates neurodegenerative stress. *Proc Natl Acad Sci U S A*. 2020.
44. Schmidt TM, Kofuji P. An isolated retinal preparation to record light response from genetically labeled retinal ganglion cells. *J Vis Exp*. 2011;47.
45. Prusky GT, Alam NM, Beekman S, Douglas RM. Rapid quantification of adult and developing mouse spatial vision using a virtual optomotor system. *Invest Ophthalmol Vis Sci*. 2004;45(12):4611–6. <https://doi.org/10.1167/iov.04-0541>.
46. Choi SW. Life is lognormal! What to do when your data does not follow a normal distribution. *Anaesthesia*. 2016;71(11):1363–6. <https://doi.org/10.1111/anae.13666>.
47. Rodriguez AR, de Sevilla Müller LP, Brecha NC. The RNA binding protein RBPMS is a selective marker of ganglion cells in the mammalian retina. *J Comp Neurol*. 2014;522(6):1411–43. <https://doi.org/10.1002/cne.23521>.
48. Coombs J, van der List D, Wang GY, Chalupa LM. Morphological properties of mouse retinal ganglion cells. *Neuroscience*. 2006;140(1):123–36. <https://doi.org/10.1016/j.neuroscience.2006.02.079>.
49. Samsam M, Mi W, Wessig C, Zielasek J, Toyka KV, Coleman MP, et al. The Wlds mutation delays robust loss of motor and sensory axons in a genetic model for myelin-related axonopathy. *J Neurosci*. 2003;23(7):2833–9. <https://doi.org/10.1523/JNEUROSCI.23-07-02833.2003>.
50. Tsao JW, Brown MC, Carden MJ, McLean WG, Perry VH. Loss of the compound action potential: an electrophysiological, biochemical and morphological study of early events in axonal degeneration in the C57BL/Ola mouse. *Eur J Neurosci*. 1994;6(4):516–24. <https://doi.org/10.1111/j.1460-9568.1994.tb00295.x>.
51. Fischer RA, Risner ML, Roux AL, Wareham LK, Sappington RM. Impairment of membrane repolarization accompanies axon transport deficits in Glaucoma. *Front Neurosci*. 2019;13:1139. <https://doi.org/10.3389/fnins.2019.01139>.
52. Beirowski B, Babetto E, Coleman MP, Martin KR. The Wlds gene delays axonal but not somatic degeneration in a rat glaucoma model. *Eur J Neurosci*. 2008;28(6):1166–79. <https://doi.org/10.1111/j.1460-9568.2008.06426.x>.
53. Oyeboode OR, Hartley R, Singhotia J, Thomson D, Ribchester RR. Differential protection of neuromuscular sensory and motor axons and their endings in Wld(S) mutant mice. *Neuroscience*. 2012;200:142–58. <https://doi.org/10.1016/j.neuroscience.2011.10.020>.
54. Brown R, Hynes-Allen A, Swan AJ, Dissanayake KN, Gillingwater TH, Ribchester RR. Activity-dependent degeneration of axotomized neuromuscular synapses in Wld S mice. *Neuroscience*. 2015;290:300–20. <https://doi.org/10.1016/j.neuroscience.2015.01.018>.
55. Coleman MP, Höke A. Programmed axon degeneration: from mouse to mechanism to medicine. *Nat Rev Neurosci*. 2020;21(4):183–96. <https://doi.org/10.1038/s41583-020-0269-3>.
56. Gilley J, Ribchester RR, Coleman MP. Sarm1 deletion, but not Wld(S), confers lifelong Rescue in a Mouse Model of severe Axonopathy. *Cell Rep*. 2017;21(1):10–6. <https://doi.org/10.1016/j.celrep.2017.09.027>.

Publisher's Note

Springer Nature remains neutral with regard to jurisdictional claims in published maps and institutional affiliations.

Ready to submit your research? Choose BMC and benefit from:

- fast, convenient online submission
- thorough peer review by experienced researchers in your field
- rapid publication on acceptance
- support for research data, including large and complex data types
- gold Open Access which fosters wider collaboration and increased citations
- maximum visibility for your research: over 100M website views per year

At BMC, research is always in progress.

Learn more biomedcentral.com/submissions

